
Robust Out-of-distribution Detection for Neural Networks

Jiefeng Chen¹ Yixuan Li² Xi Wu³ Yingyu Liang¹ Somesh Jha¹

¹ University of Wisconsin-Madison ² Stanford University ³ Google

jchen662@wisc.edu sharonli@cs.stanford.edu wu.andrew.xi@gmail.com
{yliang, jha}@cs.wisc.edu

Abstract

Detecting anomalous inputs is critical for safely deploying deep learning models in the real world. Existing approaches for detecting out-of-distribution (OOD) examples work well when evaluated on natural samples drawn from a sufficiently different distribution than the training data distribution. However, in this paper, we show that existing detection mechanisms can be extremely brittle when evaluating on inputs with minimal adversarial perturbations which don't change their semantics. Formally, we extensively study the problem of *Robust Out-of-Distribution Detection* on common OOD detection approaches, and show that state-of-the-art OOD detectors can be easily fooled by adding small perturbations to the inputs. To counteract these threats, we propose an effective algorithm called ALOE, which performs robust training by exposing the model to both adversarially crafted inlier and outlier examples. Our method can be flexibly combined with, and render existing methods robust. On common benchmark datasets, we show that ALOE substantially improves the robustness of state-of-the-art OOD detection, with 58.4% AUROC improvement on CIFAR-10 and 46.59% improvement on CIFAR-100. Finally, we provide theoretical analysis for our method, further justifying the empirical results above.

1 Introduction

Machine learning models typically perform well when the training and testing data are sampled independently and identically from the same distribution. However, models in deployment can fail in catastrophic ways when the test data distribution differs from the distribution of the training data. In particular, high-capacity neural networks can wrongly classify inputs from unknown classes (i.e., *out-of-distribution*) into known classes with high confidence, which could have extremely high cost. For example, a traffic sign classification model used for autonomous driving systems may predict label "speed-limit-100" with high confidence for an anomalous scene without any traffic sign. This can trigger wrong actions for the car and cause unanticipated and potentially catastrophic events. Therefore, detecting autonomous OOD examples has recently been recognized as an important building block for trustworthy AI (Amodei et al., 2016).

Several previous works address this problem by relying on the raw softmax score (Hendrycks & Gimpel, 2016), the calibrated softmax score (Liang et al., 2017; Guo et al., 2017), or the Mahalanobis distance based confidence score (Lee et al., 2018) derived from a neural network. These approaches have been demonstrated to work well when evaluated on OOD images that are sampled from a sufficiently different distribution than the training distribution. However, in this paper, we argue about their inadequacy of their evaluation methods, and demonstrate that we can adversarially construct images by adding minimal semantic-preserving perturbations which can cause failure in existing OOD detectors, as illustrated in Figure 1.

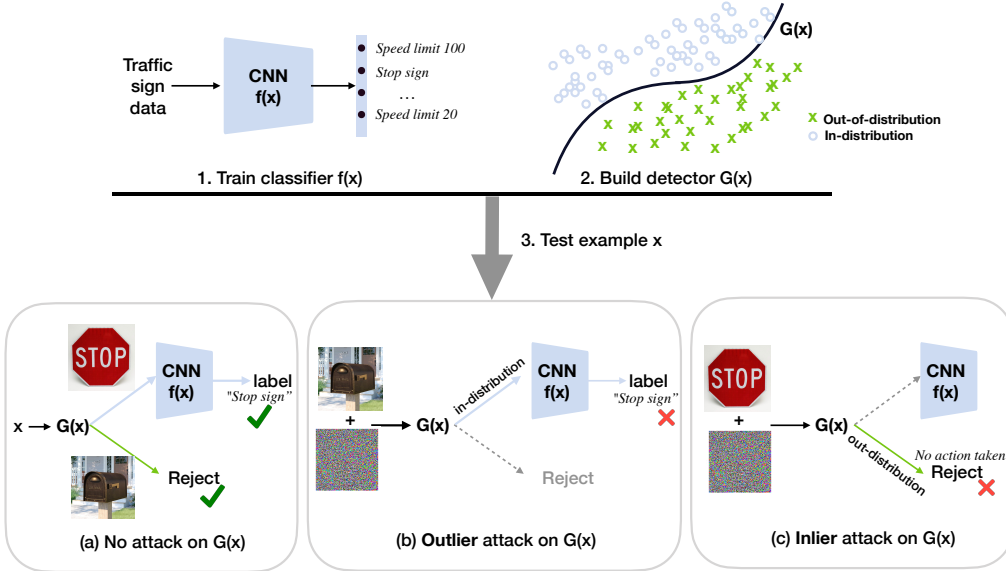


Figure 1: When deploying OOD detector $G(x)$ in the real world, there can be two types of attacks: outlier attack and inlier attack on $G(x)$. To perform outlier attack, we add small perturbation to an OOD input (e.g. mailbox) which causes the OOD detector to misclassify them as in-distribution example. The downstream classifier $f(x)$ will then classify this example into one of the known classes (e.g. stop sign), and trigger wrong action. To perform inlier attack, we add small perturbation to an in-distribution sample (e.g. stop sign) which causes the OOD detector to misclassify them as out-of-distribution example and reject it without taking the correct action (e.g. stop sign). Solid lines indicate the actual computation flow.

Formally, we study the problem of *robust out-of-distribution detection* and reveal the lack of robustness of common OOD detection methods. We show that existing OOD detection algorithms can be easily attacked to produce mistaken OOD prediction under small adversarial perturbations (Papernot et al., 2016; Goodfellow et al., 2014; Biggio et al., 2013; Szegedy et al., 2013). Specifically, we construct adversarial test examples by adding minimal perturbations so to change the model confidence in the reverse direction. We generate *adversarial in-distribution examples* such that the model is induced to produce low confidence scores; whereas *adversarial OOD examples* are constructed to induce the model to produce high confidence scores. Different from the common notion, the adversarial examples in our work are meant to fool the OOD detectors $G(x)$, rather than the original image classification model $f(x)$. It is also worth noting that the perturbation is sufficiently small so that the visual semantics as well as true distributional membership remain the same. Yet worryingly, state-of-the-art OOD detectors can fail to distinguish the samples under such adversarial attacks. Scant attention has been paid to making the OOD detectors robust against minimal input perturbations. Schwag et al. showed there exist adversarial OOD examples in settings where OOD detection is performed by having an additional background class in the image classifier $f(x)$. Our setting is different in that we treat OOD detector $G(x)$ as a separate binary classifier from $f(x)$, and therefore $G(x)$ does not interfere with the classification of known classes. In addition, the consideration of adversarial in-distribution example is also new to our work.

To address the challenge, we propose an effective method, ALOE, that improves the robust OOD detection performance. Specifically, we perform robust training by exposing the model to two types of perturbed adversarial examples. For in-distribution training data, we create a perturbed example by searching in its ϵ -ball that maximizes the negative log likelihood. In addition, we also utilize an auxiliary unlabeled dataset as in Hendrycks et al. (2018), and create corresponding perturbed outlier example by searching in its ϵ -ball that maximizes the KL-divergence between model output and a uniform distribution. The overall training objective of ALOE can be viewed as an adversarial min-max game. We show that on several benchmark datasets, ALOE can improve the robust OOD detection performance by up to 58.4% compared to previous state-of-the-art method. Our approach can be complemented by techniques such as ODIN (Liang et al., 2017), and further boost the performance.

We provide analysis and theoretical intuitions for our method. We show that training with perturbed examples from the unlabeled data helps calibrate the error on outliers from an unseen distribution, as long as the unlabeled data distribution and the new outlier distribution have a small divergence with-respect-to (w.r.t.) the hypothesis.

Our main contributions are as follows:

- We extensively examine the robust out-of-distribution detection problem on common OOD detection approaches. We show that state-of-the-art OOD detectors can fail catastrophically under small adversarial perturbations;
- We propose an effective algorithm, ALOE, that substantially improves the robustness of OOD detectors;
- We empirically analyze our method under different settings and optimization objectives, and provide theoretical insights of our approach.
- We release a code base that integrates the most common OOD detection baselines, and our robust OOD detection methods at: <https://github.com/jfc43/robust-ood-detection>. We hope this can ensure reproducibility of all methods, and make it easy for the community to conduct future research on this topic.

2 Related Work

Out-of-Distribution Detection. Various papers (Hendrycks & Gimpel, 2016; Lakshminarayanan et al., 2017; Hein et al., 2019) have reported that discriminative neural networks can produce overconfident predictions on out-of-distribution inputs. Liang et al. propose a method which can improve performance of OOD detectors using calibrated score (Guo et al., 2017). In addition, they make the maximum softmax probability more discriminative between out-of-distribution and in-distribution examples by pre-processing input data with small perturbations. Some methods also modify the neural networks by re-training or fine-tuning on some auxiliary anomalous data that are or realistic (Hendrycks et al., 2018; Mohseni et al., 2020) or artificially generated by GANs (Lee et al., 2017). Many other works (Subramanya et al., 2017; Malinin & Gales, 2018; Bevandić et al., 2018) also regularize the model to have lower confidence on anomalous examples. Worst-case aspects of OOD detection have previously been studied in (Hein et al., 2019; Meinke & Hein, 2019; Schwag et al., 2019). However, these papers are primarily concerned with adversarial out-of-distribution examples. We are the first to present a unified framework to study both adversarial inlier and outlier problems.

Density Estimation. Generative models (Dinh et al., 2016; Kingma & Welling, 2013; Rezende et al., 2014; Van den Oord et al., 2016; Tabak & Turner, 2013) can be alternative approaches for detecting OOD examples, as they directly estimate the in-distribution density and can declare a test sample to be out-of-distribution if it lies in the low-density regions. However, as shown by Nalisnick et al., deep generative models can assign a high likelihood to out-of-distribution data, which urges caution against using deep generative models to detect out-of-distribution inputs. Yet, deep generative models can detect out-of-distribution inputs when using alternative metrics (Choi & Jang, 2018), likelihood ratio (Ren et al., 2019; Serrà et al., 2019), and modified training technique (Hendrycks et al., 2018). Recently, Pope et al. show that flow-based generative models are extremely sensitive to two types of adversarial attacks: one that minimizes the likelihood scores of in-distribution samples, while the other that maximizes the likelihood scores of out-of-distribution ones.

Adversarial Robustness. Although the detectors based on deep models perform quite well on many OOD detection tasks, they might not be robust against minimal input perturbations since the behaviors of neural networks have been showed to be very brittle if we add small perturbations to the inputs. A well-known phenomenon of adversarial examples (Goodfellow et al., 2014) has received great attention in recent years. Many defense methods have been proposed to address this problem. One of the most effective methods is adversarial training (Madry et al., 2017) which uses robust optimization techniques to render deep learning models resistant to adversarial attacks. Another brittleness of deep learning models is their interpretation is fragile (Ghorbani et al., 2019): adding small input perturbations will make deep learning models generate totally different explanations for their predictions while maintaining their correct predictions. A method called robust attribution regularization (Chen et al., 2019), which also uses robust optimization, is proposed to solve this problem. In this paper, we show that the OOD detectors built from deep models are also very brittle

under small perturbations, and propose a method to mitigate this issue using techniques from robust optimization.

3 Preliminaries

In this section, we will introduce the traditional OOD detection problem and existing approaches.

3.1 Traditional Out-of-Distribution Detection Problem

OOD detection can be formulated as a canonical binary classification problem. Suppose we have an **in-distribution** $P_{\mathbf{X}}$ defined on an input space $\mathcal{X} \subset \mathbb{R}^n$. An OOD classifier $G : \mathcal{X} \mapsto \{0, 1\}$ is built to distinguish whether an input x is from $P_{\mathbf{X}}$ (give it label 1) or not (give it label 0).

In testing, the detector G is evaluated on inputs drawn from a mixture distribution $\mathcal{M}_{\mathbf{X} \times Z}$ defined on $\mathcal{X} \times \{0, 1\}$, where the conditional probability distributions $\mathcal{M}_{\mathbf{X}|Z=1} = P_{\mathbf{X}}$ and $\mathcal{M}_{\mathbf{X}|Z=0} = Q_{\mathbf{X}}$. We assume that Z is drawn uniformly from $\{0, 1\}$. $Q_{\mathbf{X}}$ is also a distribution defined on \mathcal{X} which we refer to it as **out-distribution**. We use Wasserstein distance $W_d(P_{\mathbf{X}}, Q_{\mathbf{X}})$ to measure the distance between two distributions $P_{\mathbf{X}}$ and $Q_{\mathbf{X}}$, where $d(\cdot, \cdot)$ is a distance metric. We say $P_{\mathbf{X}}$ and $Q_{\mathbf{X}}$ are sufficiently different if $W_d(P_{\mathbf{X}}, Q_{\mathbf{X}}) > \rho$, where ρ is a positive constant. We have an assumption that $P_{\mathbf{X}}$ and $Q_{\mathbf{X}}$ are sufficiently different. We denote by $\mathcal{D}_{\text{in}}^{\text{test}}$ an in-distribution test set drawn from $P_{\mathbf{X}}$, and $\mathcal{D}_{\text{out}}^{\text{test}}$ an out-of-distribution test set drawn from $Q_{\mathbf{X}}$. The *detection error* of $G(x)$ evaluated under in-distribution $P_{\mathbf{X}}$ and out-distribution $Q_{\mathbf{X}}$ is defined by

$$L(P_{\mathbf{X}}, Q_{\mathbf{X}}; G) = \frac{1}{2} (\mathbb{E}_{x \sim P_{\mathbf{X}}} \mathbb{I}[G(x) = 0] + \mathbb{E}_{x \sim Q_{\mathbf{X}}} \mathbb{I}[G(x) = 1]) \quad (1)$$

In practice, it can be intractable to directly minimize $L(P_{\mathbf{X}}, Q_{\mathbf{X}}; G)$ due to lack of prior knowledge on $Q_{\mathbf{X}}$. In some cases we assume having access to auxiliary data sampled from a distribution $U_{\mathbf{X}}$ which is different from both $P_{\mathbf{X}}$ and $Q_{\mathbf{X}}$.

3.2 Existing Approaches

Recently, several approaches propose to detect OOD examples based on different notions of confidence scores from a neural network $f(\cdot)$, which is trained on a dataset $\mathcal{D}_{\text{in}}^{\text{train}}$ drawn from a data distribution $P_{\mathbf{X}, Y}$ defined on $\mathcal{X} \times \mathcal{Y}$ with $\mathcal{Y} = \{1, 2, \dots, K\}$. Note that $P_{\mathbf{X}}$ is the marginal distribution of $P_{\mathbf{X}, Y}$. Based on this notion, we describe a few common methods below.

Maximum Softmax Probability (MSP). Maximum Softmax Probability method is as a common baseline for OOD detection (Hendrycks & Gimpel, 2016). Given an input image x and a pre-trained neural network $f(\cdot)$, the softmax output of the classifier is computed by

$$F(x) = \frac{e^{f_i(x)}}{\sum_{j=1}^K e^{f_j(x)}}.$$

A threshold-based detector $G(x)$ relies on the confidence score $S(x; f) = \max_i F_i(x)$ to make prediction as follows

$$G_{\text{MSP}}(x; \gamma, f) = \begin{cases} 0 & \text{if } S(x; f) \leq \gamma \\ 1 & \text{if } S(x; f) > \gamma \end{cases} \quad (2)$$

where γ is the confidence threshold.

ODIN. The original softmax confidence scores used in Hendrycks & Gimpel (2016) can be over-confident. ODIN (Liang et al., 2017) leverages this insight and improves the MSP baseline using the calibrated confidence score instead (Guo et al., 2017). Specifically, the calibrated confidence score is computed by

$$S(x; T, f) = \max_i \frac{e^{f_i(x)/T}}{\sum_{j=1}^K e^{f_j(x)/T}},$$

where $T \in \mathbb{R}^+$ is a temperature scaling parameter. In addition, ODIN applies small noise perturbation to the inputs

$$\tilde{x} = x - \eta \cdot \text{sign}(-\nabla_x \log S(x; T, f)), \quad (3)$$

where the parameter η is the perturbation magnitude.

By combining the two components together, ODIN detector G_{ODIN} is given by

$$G_{\text{ODIN}}(x; T, \eta, \gamma, f) = \begin{cases} 0 & \text{if } S(\tilde{x}; T, f) \leq \gamma \\ 1 & \text{if } S(\tilde{x}; T, f) > \gamma \end{cases} \quad (4)$$

In real applications, it may be difficult to know the out-of-distribution samples one will encounter in advance. The hyperparameters of T and η can be tuned instead on a random noise data such as Gaussian or uniform distribution, without requiring prior knowledge of OOD dataset.

Mahalanobis. Lee et al. model the features of training data as class-conditional Gaussian distribution, where its parameters are chosen as empirical class means and empirical covariance of training samples. Specifically, for a given sample x , the confidence score from the ℓ -th feature layer is defined using the Mahalanobis distance with respect to the closest class-conditional distribution:

$$M_\ell(x) = \max_c -(f_\ell(x) - \hat{\mu}_{\ell,c})^T \hat{\Sigma}_\ell^{-1} (f_\ell(x) - \hat{\mu}_{\ell,c}), \quad (5)$$

where $f_\ell(x)$ is the ℓ -th hidden features of DNNs, and $\hat{\mu}_{\ell,c}$ and $\hat{\Sigma}_\ell$ are the empirical class means and covariances computed from the training data respectively.

In addition, they use two techniques (1) input pre-processing and (2) feature ensemble. Specifically, for each test sample x , they first calculate the pre-processed sample \tilde{x}_ℓ by adding the small perturbations as in Liang et al. (2017):

$$\tilde{x}_\ell = x + \eta \cdot \text{sign}(\nabla_x M_\ell(x)), \quad (6)$$

where η is a magnitude of noise, which can be tuned on the validation data.

The confidence scores from all layers are integrated through a weighted averaging: $\sum_\ell \alpha_\ell M_\ell(\tilde{x}_\ell)$. The weight of each layer α_ℓ is learned through a logistic regression model, which predicts 1 for in-distribution and 0 for OOD examples. The overall Mahalanobis distance based confidence score is

$$M(x) = \frac{1}{1 + e^{-(\sum_\ell \alpha_\ell M_\ell(\tilde{x}_\ell) + b)}}, \quad (7)$$

where b is the bias of the logistic regression model. Putting it all together, the final Mahalanobis detector $G_{\text{Mahalanobis}}$ is given by

$$G_{\text{Mahalanobis}}(x; \eta, \gamma, \{\alpha_\ell\}, b, f) = \begin{cases} 0 & \text{if } M(x) \leq \gamma \\ 1 & \text{if } M(x) > \gamma \end{cases} \quad (8)$$

Outlier Exposure (OE). Outlier Exposure (Hendrycks et al., 2018) makes use of a large, unlabeled auxiliary dataset $\mathcal{D}_{\text{out}}^{\text{OE}}$ drawn from U_X to improve out-of-distribution detection. A new classifier, F_{OE} , parameterized by θ , is trained using the following objective

$$\underset{\theta}{\text{minimize}} \quad \mathbb{E}_{(x,y) \sim \mathcal{D}_{\text{in}}^{\text{train}}} [-\log F_y(x)] + \lambda \cdot \mathbb{E}_{x \sim \mathcal{D}_{\text{out}}^{\text{OE}}} [L_{\text{CE}}(F(x), \mathcal{U}_K)],$$

where $F(\cdot)$ is softmax output of the classification model trained on $P_{X,Y}$, and \mathcal{U}_K is the uniform distribution over K classes. The cross-entropy loss $L_{\text{CE}}(z, y) = -\sum_{i=1}^K y_i \log z_i$. This objective regularizes the model F to produce more conservative predictions (uncertainties) on the out-of-distribution samples. The classifier F_{OE} can be combined with downstream OOD detection methods (such as MSP or ODIN). The corresponding detectors can be constructed as $G_{\text{MSP}}(x; \gamma, F_{\text{OE}})$, and $G_{\text{ODIN}}(x; T, \eta, \gamma, F_{\text{OE}})$, respectively.

4 Robust Out-of-Distribution Detection

Traditional OOD detection methods described in Section 3.2 are shown to work well when evaluated on natural images that are sampled from a sufficiently different distribution than the training data distribution. However, in this section, we show that existing OOD detectors are extremely brittle and can fail when we add minimal semantic-preserving perturbations to the inputs. We start by formally describing the problem of *robust out-of-distribution detection*.

Problem Statement. We define $\Omega(x)$ to be a set of semantic-preserving perturbations on an input x . For $\delta \in \Omega(x)$, $x + \delta$ has the same semantic label as x . This also means that x and $x + \delta$ have the same distributional membership (i.e. x and $x + \delta$ both belong to in-distribution P_X , or out-distribution Q_X).

A robust OOD classifier $G : \mathcal{X} \mapsto \{0, 1\}$ is built to distinguish whether a perturbed input $x + \delta$ is from P_X or not. In testing, the detector G is evaluated on perturbed inputs drawn from a mixture distribution $\mathcal{M}_{X \times Z}$ defined on $\mathcal{X} \times \{0, 1\}$, where the conditional probability distributions $\mathcal{M}_{X|Z=1} = P_X$ and $\mathcal{M}_{X|Z=0} = Q_X$. We assume that Z is drawn uniformly from $\{0, 1\}$ and P_X is sufficiently different from Q_X . The *detection error* of G evaluated under in-distribution P_X and out-distribution Q_X is now defined by

$$L(P_X, Q_X; G, \Omega) = \frac{1}{2} (\mathbb{E}_{x \sim P_X} \max_{\delta \in \Omega(x)} \mathbb{I}[G(x + \delta) = 0] + \mathbb{E}_{x \sim Q_X} \max_{\delta \in \Omega(x)} \mathbb{I}[G(x + \delta) = 1]) \quad (9)$$

In practice, it can be intractable to directly minimize $L(P_X, Q_X; G, \Omega)$ due to lack of prior knowledge on Q_X . In some cases we assume having access to auxiliary data sampled from a distribution U_X which is different from both P_X and Q_X .

Adversarial Attacks on OOD Detection. We describe adversarial attack algorithms that can show the vulnerability of existing OOD detection approaches. Computing the exact value of detection error defined in equation (9) requires enumerating all possible perturbations. This can be practically intractable given the large space of $\Omega(x) \subset \mathbb{R}^n$. To this end, we propose adversarial attack algorithms that can find the perturbations in $\Omega(x)$ to compute a lower bound.

Specifically, we consider image data and small L_∞ norm-bounded perturbations on x since it is commonly used in adversarial machine learning research (Madry et al., 2017; Athalye et al., 2018). For data point $x \in \mathbb{R}^n$, a set of adversarial perturbations is defined as

$$B(x, \epsilon) = \{\delta \in \mathbb{R}^n \mid \|\delta\|_\infty \leq \epsilon \wedge x + \delta \text{ is valid}\}, \quad (10)$$

where ϵ is the size of small perturbation, which is also called adversarial budget. $x + \delta$ is considered valid if the values of $x + \delta$ are in the image pixel value range.

For the OOD detection methods based on softmax confidence score (e.g. MSP, ODIN and OE), we describe the attack mechanism in Algorithm 1. Specifically, we construct adversarial test examples by adding small perturbations in $B(x, \epsilon)$ so to change the prediction confidence in the reverse direction. To generate *adversarial in-distribution examples*, the model is induced to output probability distribution that is close to uniform; whereas *adversarial OOD examples* are constructed to induce the model produce high confidence score. We note here that the adversarial examples here are constructed to fool the OOD detectors $G(x)$, rather than the image classification model $f(x)$.

Algorithm 1 Adversarial attack on OOD detectors based on softmax confidence score.

input x, F, ϵ, m, ξ

output δ

$\delta \leftarrow$ randomly choose a vector from $B(x, \epsilon)$

for $t = 1, 2, \dots, m$ **do**

$x' \leftarrow x + \delta$

if x is in-distribution **then**

$\ell(x') \leftarrow L_{\text{CE}}(F(x'), \mathcal{U}_K)$

else

$\ell(x') \leftarrow -\sum_{i=1}^K F_i(x') \log F_i(x')$

end if

$\delta' \leftarrow \delta - \xi \cdot \text{sign}(\nabla_x \ell(x'))$

$\delta \leftarrow \prod_{B(x, \epsilon)} \delta'$

\triangleright projecting δ' to $B(x, \epsilon)$

end for

For the OOD detection methods using Mahalanobis distance based confidence score, we propose an attack algorithm detailed in Algorithm 2. Specifically, we construct adversarial test examples by adding small perturbations in $B(x, \epsilon)$ to make the logistic regression detector predict wrongly.

Algorithm 2 Adversarial attack on OOD detector using Mahalanobis distance based confidence score.

input $x, M_\ell(\cdot), \{\alpha_\ell\}, b, \epsilon, m, \xi$
output δ
 $\delta \leftarrow$ randomly choose a vector from $B(x, \epsilon)$
for $t = 1, 2, \dots, m$ **do**
 $x' \leftarrow x + \delta$
 $p(x') \leftarrow \frac{1}{1 + e^{-(\sum_\ell \alpha_\ell M_\ell(x') + b)}}$
if x is in-distribution **then**
 $\ell(x') \leftarrow -\log p(x')$
else
 $\ell(x') \leftarrow -\log(1 - p(x'))$
end if
 $\delta' \leftarrow \delta + \xi \cdot \text{sign}(\nabla_x \ell(x'))$
 $\delta \leftarrow \prod_{B(x, \epsilon)} \delta'$ \triangleright projecting δ' to $B(x, \epsilon)$
end for

Note that in our attack algorithm, we don't perform input pre-processing to compute the Mahalanobis distance based confidence score.

Our attack algorithms assume having access to the model parameters, thus they are white-box attacks. We find that using our attack algorithms, even with very minimal attack strength ($\epsilon = 1/255$ and $m = 10$), classic OOD detection methods (e.g. MSP, ODIN, Mahalanobis, OE, and OE+ODIN) can fail miserably. For example, the false positive rate of OE method can increase by 95.52% under such attack when evaluated on CIFAR-10 as in-distribution dataset. We provide experimental results in more detail in Section 6.

5 ALOE: Adversarial Learning with inlier and Outlier Exposure

In this section, we introduce a novel method called *Adversarial Learning with inlier and Outlier Exposure (ALOE)* to improve the robustness of the OOD detector $G(\cdot)$ built on top of the neural network $f(\cdot)$ against input perturbations.

Training Objective. We train our model ALOE against two types of perturbed examples. For in-distribution inputs $x \in P_X$, ALOE creates *adversarial inlier* within the ϵ -ball that maximize the negative log likelihood. Training with perturbed examples from the in-distribution helps calibrate the error on inliers, and make the model more invariant to the additive noise. In addition, our method leverages an auxiliary unlabeled dataset $\mathcal{D}_{\text{out}}^{\text{OE}}$ drawn from U_X as used in Hendrycks et al. (2018), but in a different objective. While OE directly uses the original images $x \in \mathcal{D}_{\text{out}}^{\text{OE}}$ as outliers, ALOE creates *adversarial outliers* by searching within the ϵ -ball that maximize the KL-divergence between model output and a uniform distribution. The overall training objective of F_{ALOE} can be formulated as a min-max game given by

$$\underset{\theta}{\text{minimize}} \quad \mathbb{E}_{(x,y) \sim \mathcal{D}_{\text{in}}^{\text{train}}} \max_{\delta \in B(x, \epsilon)} [-\log F_\theta(x + \delta)_y] + \lambda \cdot \mathbb{E}_{x \sim \mathcal{D}_{\text{out}}^{\text{OE}}} \max_{\delta \in B(x, \epsilon)} [L_{\text{CE}}(F_\theta(x + \delta), \mathcal{U}_K)]$$

where $F_\theta(x)$ is the softmax output of the neural network.

To solve the inner max of these objectives, we use the Projected Gradient Descent (PGD) method (Madry et al., 2017), which is the standard method for large-scale constrained optimization. The hyper-parameters of PGD used in the training will be provided in the experiments.

Once the model F_{ALOE} is trained, it can be used for downstream OOD detection by combining with approaches such as MSP and ODIN. The corresponding detectors can be constructed as $G_{\text{MSP}}(x; \gamma, F_{\text{ALOE}})$, and $G_{\text{ODIN}}(x; T, \eta, \gamma, F_{\text{ALOE}})$, respectively.

Possible Variants. We also derive two other variants of robust training objective for OOD detection. The first one performs adversarial training *only* on the inliers. We denote this method as ADV, which

is equivalent to the objective used in [Madry et al. \(2017\)](#).

$$\underset{\theta}{\text{minimize}} \quad \mathbb{E}_{(x,y) \sim \mathcal{D}_{\text{in}}^{\text{train}}} \max_{\delta \in B(x,\epsilon)} [-\log F_{\theta}(x + \delta)_y]$$

Alternatively, we also considered performing adversarial training on inlier examples while simultaneously performing outlier exposure as in [Hendrycks et al. \(2018\)](#). We refer to this variant as AOE (adversarial learning with outlier exposure).

$$\underset{\theta}{\text{minimize}} \quad \mathbb{E}_{(x,y) \sim \mathcal{D}_{\text{in}}^{\text{train}}} \max_{\delta \in B(x,\epsilon)} [-\log F_{\theta}(x + \delta)_y] + \lambda \cdot \mathbb{E}_{x \sim \mathcal{D}_{\text{out}}^{\text{OE}}} [L_{\text{CE}}(F_{\theta}(x), \mathcal{U}_K)]$$

We provide ablation studies comparing these variants with ALOE in Section 6.

6 Experiments

In this section we perform experiments to answer the following questions:

- (Q1) Are classic OOD detection methods (e.g. MSP, ODIN, Mahalanobis, and OE) robust against semantic-preserving input perturbations?
- (Q2) How does ALOE perform on the robust OOD detection task and the original classification task, compared to existing approaches?
- (Q3) How will the hyper-parameters such as adversarial budget ϵ affect the experimental results?

We perform extensive experiments to answer these questions. In summary, we have the following findings:

- (A1) Classic OOD detection methods such as ODIN, Mahalanobis, and OE fail drastically under our adversarial attack even with a very small attack budget.
- (A2) Our method ALOE can significantly improve the performance of OOD detection under our adversarial attack compared to the classic OOD detection methods. Also, we observe that the performance of its variants ADV and AOE is worse than it in this task. And if we combine ALOE with other OOD detection approaches such as ODIN, we can further improve its performance. What’s more, ALOE improves model robustness while maintaining almost the same classification accuracy on clean inputs.
- (A3) When we increase the adversarial budget ϵ , the attack will be stronger and the robust OOD detection performance decreases for classic methods. ALOE consistently improves the performance under different attack strengths.

Next we provide more details.

6.1 Setup

In-distribution Datasets. we use GTSRB ([Stallkamp et al., 2012](#)), CIFAR-10 and CIFAR-100 datasets ([Krizhevsky et al., 2009](#)) as in-distribution datasets. The pixel values of all the images are normalized to be in the range [0,1]. The details of these datasets can be found in the appendix B.1.

Out-of-distribution Datasets. For auxiliary outlier dataset, we use 80 Million Tiny Images ([Torralba et al., 2008](#)), which is a large-scale, diverse dataset scraped from the web. We follow the same deduplication procedure as in [Hendrycks et al. \(2018\)](#) and remove all examples in this dataset that appear in CIFAR-10 and CIFAR-100 to ensure that $\mathcal{D}_{\text{out}}^{\text{OE}}$ and $\mathcal{D}_{\text{out}}^{\text{test}}$ are disjoint. For OOD test dataset, we follow the settings in [Liang et al. \(2017\)](#); [Hendrycks et al. \(2018\)](#). For CIFAR-10 and CIFAR-100, we use six different natural image datasets: SVHN, Textures, Places365, LSUN (crop), LSUN (resize), and iSUN. For GTSRB, we use the following six datasets that are sufficiently different from it: CIFAR-10, Textures, Places365, LSUN (crop), LSUN (resize), and iSUN. Again, the pixel values of all the images are normalized to be in the range [0,1]. The details of these datasets can be found in the appendix B.1.

Architectures and Training Configurations. We use the state-of-the-art neural network architecture DenseNet ([Huang et al., 2017](#)). We follow the same setup as in [Huang et al. \(2017\)](#), with depth $L = 100$, growth rate $k = 12$ (Dense-BC) and dropout rate 0. All neural networks are trained with

stochastic gradient descent with Nesterov momentum (Duchi et al., 2011; Kingma & Ba, 2014). Specifically, we train Dense-BC with momentum 0.9 and ℓ_2 weight decay with a coefficient of 10^{-4} . For GTSRB, we train it for 10 epochs; for CIFAR-10 and CIFAR-100, we train it for 100 epochs. For in-distribution dataset, we use batch size 64; For outlier exposure with $\mathcal{D}_{\text{out}}^{\text{OE}}$, we use batch size 128. The initial learning rate of 0.1 decays following a cosine learning rate schedule (Loshchilov & Hutter, 2016).

Hyperparameters. For ODIN (Liang et al., 2017), we choose temperature scaling parameter T and perturbation magnitude η by validating on a random noise data, which does not depend on prior knowledge of out-of-distribution datasets in test. In all of our experiments, we set $T = 1000$. We set $\eta = 0.0004$ for GTSRB, $\eta = 0.0014$ for CIFAR-10, and $\eta = 0.0028$ for CIFAR-100. For Mahalanobis (Lee et al., 2018), we randomly select 1,000 examples from $\mathcal{D}_{\text{in}}^{\text{train}}$ and 1,000 examples from $\mathcal{D}_{\text{out}}^{\text{OE}}$ to train the Logistic Regression model and tune η , where η is chosen from 21 evenly spaced numbers starting from 0 and ending at 0.004, and the optimal parameters are chosen to minimize the FPR at TPR 95%. For OE, AOE and ALOE methods, we fix the regularization parameter λ to be 0.5. In PGD that solves the inner max of ADV, AOE and ALOE, we use step size $1/255$, number of steps $\lfloor 255\epsilon + 1 \rfloor$, and random start. For our attack algorithm, we set $\xi = 1/255$ and $m = 10$ in our experiments. The adversarial budget ϵ by default is set to $1/255$, however we perform ablation studies by varying the value.

More experiment settings can be found in the Appendix B.1.

6.2 Evaluation Metrics

We report main results using three metrics described below. In addition, we also evaluate our method using AURP metric, which is described in Appendix B.2.

FPR at 95% TPR. This metric calculates the false positive rate (FPR) on out-of-distribution examples when the true positive rate (TPR) is 95%.

Detection Error. This metric corresponds to the minimum mis-detection probability over all possible thresholds γ , which is $\min_{\gamma} L(P_X, Q_X; G(x; \gamma))$.

AUROC. Area Under the Receiver Operating Characteristic curve is a threshold-independent metric (Davis & Goadrich, 2006). It can be interpreted as the probability that a positive example is assigned a higher detection score than a negative example (Fawcett, 2006). A perfect detector corresponds to an AUROC score of 100%.

6.3 Results

All the values reported in this section are averaged over *six* OOD test datasets. We provide detailed results for each individual dataset in Appendix B.3.

Classic OOD detection methods fail under our attack. As shown in Table 1, although classic OOD detection methods (e.g. MSP, ODIN, Mahalanobis, OE and OE+ODIN) could perform quite well on detecting natural OOD samples, their performance drops substantially under the attack (even with very minimal attack budget ($\epsilon = 1/255$ and $m = 10$)). For the best-performing OOD detection method (i.e., OE+ODIN), the FPR at 95% TPR increases drastically from 4.17% (without attack) to 99.02% (with attack) when evaluated on the CIFAR-10 dataset.

ALOE improves robust OOD detection performance. As shown in Table 1, our method ALOE could significantly improve the OOD detection performance under the adversarial attack. For example, ALOE can substantially improve the AUROC from 34.29% (state-of-the-art: OE+ODIN) to 92.69% evaluated on the CIFAR-10 dataset. The performance can be further improved when combining ALOE with ODIN. We observe this trend holds consistently on other benchmark datasets GTSRB and CIFAR-100 as in-distribution training data. We also find that adversarial training (ADV) or combining adversarial training with outlier exposure (AOE) yield slightly less competitive results.

To better understand our method, we analyze the distribution of the confidence scores produced by the OOD detectors on SVHN (out-distribution) and CIFAR-10 (in-distribution). As shown in Figure 2, OE could distinguish in-distribution and out-of-distribution samples quite well since the confidence scores are well separated. However, under our attack, the confidence scores of in-distribution samples move towards 0 and the scores of out-of-distribution samples move towards 1.0, which renders the detector fail to distinguish in- and out-of-distribution samples. Using our method, the confidence

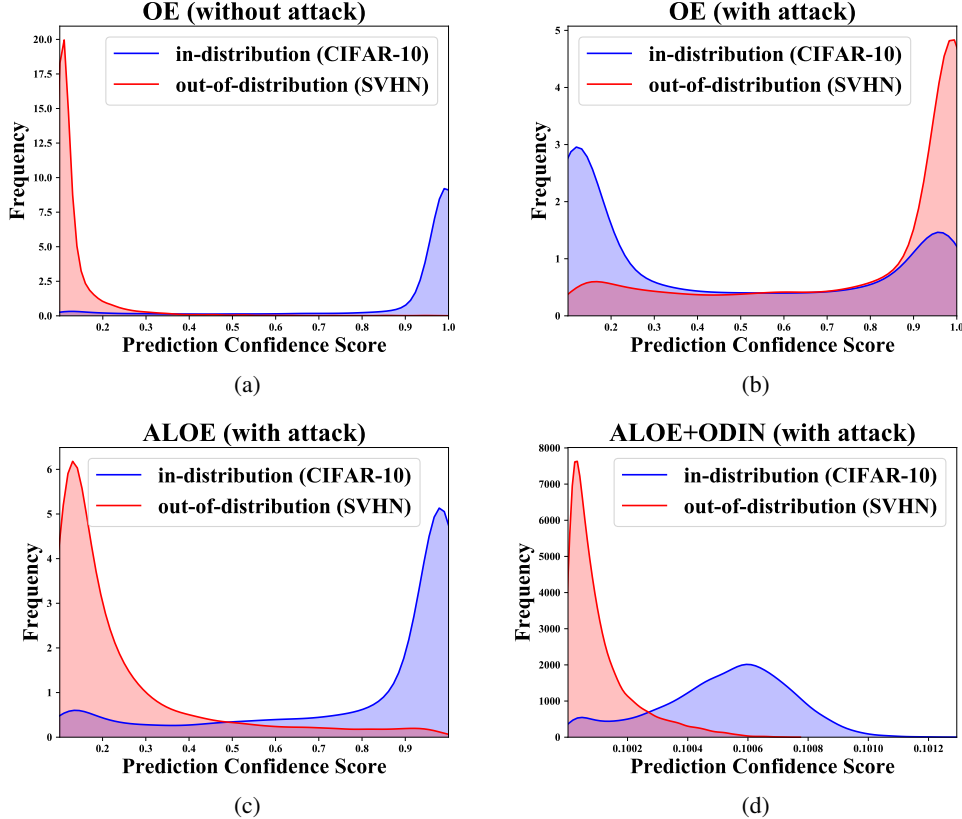


Figure 2: Confidence score distribution produced by different methods. For illustration purposes, we use CIFAR-10 as in-distribution and SVHN as out-of-distribution. (a) and (b) compare the score distribution for Outlier Exposure (Hendrycks et al., 2018), evaluated on clean images and PGD attacked images, respectively. The distribution overall shift toward the opposite direction under our attack, which causes the method to fail. Our method ALOE can mitigate the distribution shift as shown in (c). When combined with ODIN (Liang et al., 2017), the score distributions can be further separable between in- and out-distributions, as shown in (d).

scores (under attack) become separable and shift toward the right direction. If we further combine ALOE with ODIN, the scores produced by the detector are even more separated.

Effect of adversarial budget ϵ . We further perform ablation study on the adversarial budget ϵ and analyze how this affects performance. On GTSRB and CIFAR-10 dataset, we perform comparison by varying $\epsilon = 1/255, 2/255, 3/255, 4/255$. The results are reported in Table 2. We observe that as we increase ϵ , the performance on classic OOD detection methods (e.g. MSP, ODIN, Mahalanobis, OE, OE+ODIN) drops significantly under our attack: the FPR at 95% TPR reaches almost 100% for all those methods. We also observe that our methods ALOE (and ALOE+ODIN) consistently improves the results under our attack compared to those classic methods.

Classification performance of image classifier $f(x)$. In addition to OOD detection, we also verify the accuracy and robustness on the original classification task. The results are presented in table 3. *Robustness* measures the accuracy under PGD attack w.r.t the original classification model. We use adversarial budget ϵ of $1/255$ and number of attack steps of 10. *Original* refers to the vanilla model trained with standard cross entropy loss on the dataset. On both GTSRB and CIFAR-10, ALOE improves the model robustness, while maintaining almost the same classification accuracy on the clean inputs. On CIFAR-100, ALOE improves robustness from 7.29% to 55.97%, albeit dropping the classification accuracy slightly (3.64%). Overall our method achieves good trade-off between the accuracy and robustness due to adversarial perturbations.

\mathcal{D}_{in}^{test}	Method	FPR (95% TPR)	Detection Error	AUROC	FPR (95% TPR)	Detection Error	AUROC
		↓	↓	↑	↓	↓	↑
		without attack			with attack ($\epsilon = 1/255, m = 10$)		
GTSRB	MSP (Hendrycks & Gimpel, 2016)	1.13	2.42	98.45	97.59	26.02	73.27
	ODIN (Liang et al., 2017)	1.42	2.10	98.81	75.94	24.87	75.41
	Mahalanobis (Lee et al., 2018)	1.31	2.87	98.29	100.00	29.80	70.45
	OE (Hendrycks et al., 2018)	0.02	0.34	99.92	25.85	5.90	96.09
	OE+ODIN	0.02	0.36	99.92	14.14	5.59	97.18
	ADV (Madry et al., 2017)	1.45	2.88	98.66	17.96	6.95	94.83
	AOE	0.00	0.62	99.86	1.49	2.55	98.35
	ALOE (ours)	0.00	0.44	99.76	0.66	1.80	98.95
CIFAR-10	ALOE+ODIN (ours)	0.01	0.45	99.76	0.69	1.80	98.98
	MSP (Hendrycks & Gimpel, 2016)	51.67	14.06	91.61	99.98	50.00	10.34
	ODIN (Liang et al., 2017)	25.76	11.51	93.92	93.45	46.73	28.45
	Mahalanobis (Lee et al., 2018)	31.01	15.72	88.53	89.75	44.30	32.54
	OE (Hendrycks et al., 2018)	4.47	4.50	98.54	99.99	50.00	25.13
	OE+ODIN	4.17	4.31	98.55	99.02	47.84	34.29
	ADV (Madry et al., 2017)	66.99	19.22	87.23	98.44	31.72	66.73
	AOE	10.46	6.58	97.76	88.91	26.02	78.39
CIFAR-100	ALOE (ours)	5.47	5.13	98.34	53.99	14.19	91.26
	ALOE+ODIN (ours)	4.48	4.66	98.55	41.59	12.73	92.69
	MSP (Hendrycks & Gimpel, 2016)	81.72	33.46	71.89	100.00	50.00	2.39
	ODIN (Liang et al., 2017)	58.84	22.94	83.63	98.87	49.87	21.02
	Mahalanobis Lee et al. (2018)	53.75	27.63	70.85	95.79	47.53	17.92
	OE (Hendrycks et al., 2018)	56.49	19.38	87.73	100.00	50.00	2.94
	OE+ODIN	47.59	17.39	90.14	99.49	50.00	20.02
	ADV (Madry et al., 2017)	85.47	33.17	71.77	99.64	44.86	41.34
CIFAR-100	AOE	60.00	23.03	84.57	95.79	43.07	53.80
	ALOE (ours)	61.99	23.56	83.72	92.01	40.09	61.20
	ALOE+ODIN (ours)	58.48	21.38	85.75	88.50	36.20	66.61

Table 1: Distinguishing in- and out-of-distribution test set data for image classification. We contrast performance on clean images (without attack) and PGD attacked images. \uparrow indicates larger value is better, and \downarrow indicates lower value is better. All values are percentages and are averaged over six OOD test datasets mentioned in section 6.1. The detail results on each OOD test dataset can be found in Appendix B.3.

\mathcal{D}_{in}^{test}	Method	FPR (95% TPR)	Detection Error	AUROC	FPR (95% TPR)	Detection Error	AUROC	FPR (95% TPR)	Detection Error	AUROC
		↓	↓	↑	↓	↓	↑	↓	↓	↑
		with attack ($\epsilon = 2/255, m = 10$)			with attack ($\epsilon = 3/255, m = 10$)			with attack ($\epsilon = 4/255, m = 10$)		
GTSRB	MSP (Hendrycks & Gimpel, 2016)	99.88	50.00	26.11	99.99	50.00	6.79	99.99	50.00	6.39
	ODIN (Liang et al., 2017)	99.23	49.97	27.38	99.83	50.00	6.94	99.84	50.00	6.52
	Mahalanobis Lee et al. (2018)	100.00	49.97	26.37	100.00	50.00	8.27	100.00	50.00	7.82
	OE (Hendrycks et al., 2018)	96.79	16.09	83.06	99.91	25.36	68.62	99.97	26.37	66.91
	OE+ODIN	89.88	15.78	84.56	99.25	24.70	69.71	99.45	25.67	68.02
	ADV (Madry et al., 2017)	92.17	11.51	89.92	99.65	18.59	80.85	99.49	18.68	81.17
	AOE	7.94	5.36	94.82	16.16	10.38	88.72	38.05	17.95	83.84
	ALOE (ours)	4.03	4.19	95.90	10.82	7.64	91.21	16.10	10.10	89.52
CIFAR-10	ALOE+ODIN (ours)	3.95	4.15	95.72	9.56	6.91	91.08	13.85	9.22	89.44
	MSP (Hendrycks & Gimpel, 2016)	100.00	50.00	1.16	100.00	50.00	0.13	100.00	50.00	0.12
	ODIN (Liang et al., 2017)	99.73	49.99	5.67	99.98	50.00	1.14	99.99	50.00	1.06
	Mahalanobis Lee et al. (2018)	100.00	50.00	5.90	100.00	50.00	1.27	100.00	50.00	1.05
	OE (Hendrycks et al., 2018)	100.00	50.00	5.99	100.00	50.00	1.52	100.00	50.00	1.48
	OE+ODIN	100.00	50.00	8.89	100.00	50.00	2.76	100.00	50.00	2.69
	ADV (Madry et al., 2017)	99.94	36.57	56.01	99.89	39.64	49.88	99.96	40.57	48.02
	AOE	91.79	35.08	66.92	99.96	39.53	54.43	98.40	37.37	59.16
CIFAR-10	ALOE (ours)	75.90	23.36	83.26	83.14	31.54	73.46	82.53	29.92	75.52
	ALOE+ODIN (ours)	68.80	20.31	85.92	79.19	28.04	77.88	78.46	27.55	78.83

Table 2: Distinguishing in- and out-of-distribution test set data for image classification. \uparrow indicates larger value is better, and \downarrow indicates lower value is better. All values are percentages. The in-distribution datasets are GTSRB and CIFAR-10. All the values reported are averaged over six out-of-distribution test datasets described in section 6.1.

7 Analysis

The interesting questions related to our method are: (1) why unlabeled auxiliary data from U_X helps? (2) why the robustness of the detector G on U_X generalizes to a different distribution Q_X ?

To get some intuition for these questions, we adopt the domain adaption framework (Ben-David et al., 2010). Recall that in domain adaptation there are two domains s, t , each being a distribution over the input space \mathcal{X} and label space $\{0, 1\}$. A classifier is trained on s then applied on t . We view our OOD detection problem as classification, where the source domain s is P_X with labels 1 and U_X with labels 0, and the target domain t is P_X with labels 1 and Q_X with label 0.

$\mathcal{D}_{\text{in}}^{\text{test}}$	Method	Classification Accuracy	Robustness w.r.t image classifier
GTSRB	Original	99.33%	88.47%
	OE	99.38%	83.99%
	ADV	99.23%	97.13%
	AOE	98.82%	94.14%
	ALOE	98.91%	94.58%
CIFAR-10	Original	94.08%	25.38%
	OE	94.59%	28.94%
	ADV	92.97%	84.81%
	AOE	93.35%	78.60%
	ALOE	93.89%	84.02%
CIFAR-100	Original	75.26%	7.29%
	OE	74.45%	7.84%
	ADV	70.58%	54.58%
	AOE	72.56%	52.96%
	ALOE	71.62%	55.97%

Table 3: The image classification accuracy and robustness of different models on original tasks (GTSRB, CIFAR-10 and CIFAR-100). *Robustness* measures the accuracy under PGD attack w.r.t the original classification model.

Denote the loss of detector G on point (x, y) as:

$$L(G, x, y; \Omega) := \max_{\delta \in \Omega(x)} \mathbb{I}[G(x + \delta) \neq y].$$

Denote the loss of G in the source domain as:

$$R^s(G) := \frac{1}{2} \mathbb{E}_{x \sim P_X, y=1} L(G, x, y; \Omega) + \frac{1}{2} \mathbb{E}_{x \sim U_X, y=0} L(G, x, y; \Omega)$$

and similarly define the loss $R^t(G)$ of G in the target domain. Following Ben-David et al. (2010), define (a variant) of the divergence of Q_X and U_X w.r.t. the hypothesis class \mathcal{G} as

$$d_{\mathcal{G}}(Q_X, U_X) = \sup_{G, G' \in \mathcal{G}} v(G, G'; Q_X) - v(G, G'; U_X)$$

where

$$v(G, G'; D) = \mathbb{E}_{x \sim D, y=0} (L_{\Omega}(G, x, y) - L_{\Omega}(G', x, y))$$

is the loss difference of G and G' on distribution D . The divergence upper bounds the change of the hypothesis loss difference between Q_X and U_X . If it is small, then for any $G, G' \in \mathcal{G}$ where G has a smaller risk than G' in U_X , we know that G will also have a smaller (or not too larger) risk than G' in Q_X . That is, if the divergence is small, then the ranking of the hypotheses w.r.t. the loss is roughly the same in both distributions. This *rank-preserving* property thus makes sure that a good hypothesis learned in U_X will also be good for Q_X .

Now we show that, if $d_{\mathcal{G}}(Q_X, U_X)$ is small (i.e., Q_X and U_X are aligned w.r.t. the class \mathcal{G}), then a detector G with small loss in the source domain will also have small loss in the target domain.

Theorem 1. For any $G \in \mathcal{G}$,

$$R^t(G) \leq \inf_{G^* \in \mathcal{G}} R^t(G^*) + R^s(G) + \frac{1}{2} d_{\mathcal{G}}(Q_X, U_X).$$

Proof. See the Appendix A. □

The test error of the detector is bounded by three terms: the best error, the error on the training distributions, and the divergence between Q_X and U_X . Assuming that there exists a ground-truth detector with a small test error, and that the optimization can lead to a small training error, the test error is then characterized by the divergence. So in this case, as long as the rankings of the hypotheses (according to the error) on Q_X and U_X are similar, detectors learned on U_X can generalize to Q_X .

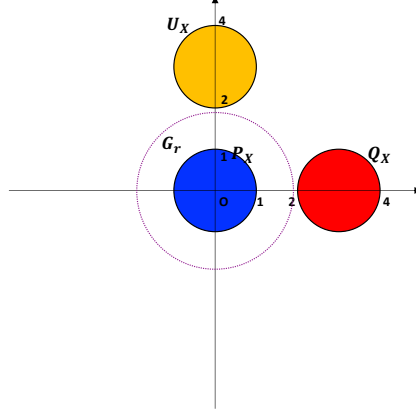


Figure 3: An illustration example to explain why U_X helps to get a good detector G_r . With U_X , we can prune away hypotheses G_r for any $r \geq 1.9$. Thus, the resulting detector G_r can detect OOD samples from Q_X successfully and robustly.

An illustration example. In this example, the in-distribution P_X is uniform over the disk around the origin in \mathbb{R}^2 with radius 1, U_X is uniform over the disk around $(0, 3)$ with radius 1, and Q_X is uniform over the disk around $(3, 0)$ with radius 1. Assume the adversary budget is $\epsilon = 0.1$, i.e., $\Omega = \{\|\delta\|_2 \leq 0.1\}$. The hypothesis class for the detector contains all functions of the form $G_r(x) = \mathbb{I}[\|x\|_2 \geq r]$ with parameter r . See Figure 3.

The example first shows the effect of the unlabeled data: U_X helps to prune away hypotheses G_r for any $r \geq 1.9$. Furthermore, it also shows how learning over U_X can generalize to Q_X . Although Q_X and U_X have non-overlapping supports, U_X help to calibrate the error of the hypotheses so that any good detector trained on P_X and U_X can be used for distinguishing P_X and Q_X . Formally, the d_G is small in Theorem 1.

The analysis also shows the importance of training on *perturbed* instances from the unlabeled data U_X . Not using perturbation is equivalent to using $\Omega = \{\mathbf{0}\}$. In this case, the analysis shows that it only guarantees the error on *unperturbed* instances from Q_X , even if Q_X and U_X has small divergence and the optimization gives small training error.

8 Conclusion

In this paper, we study the problem, Robust Out-of-Distribution Detection, and propose an adversarial attack algorithm which reveals the lack of robustness of a wide range of OOD detection methods. We show that state-of-the-art OOD detection methods can fail catastrophically under both adversarial in-distribution and out-of-distribution attacks. To counteract these threats, we propose a new method called ALOE, which substantially improves the robustness of state-of-the-art OOD detection. We empirically analyze our method under different parameter settings and optimization objectives, and provide theoretical insights behind our approach. Future work involves exploring alternative semantic-preserving perturbations beyond adversarial attacks.

References

- Dario Amodei, Chris Olah, Jacob Steinhardt, Paul Christiano, John Schulman, and Dan Mané. Concrete problems in ai safety. *arXiv preprint arXiv:1606.06565*, 2016.
- Anish Athalye, Nicholas Carlini, and David Wagner. Obfuscated gradients give a false sense of security: Circumventing defenses to adversarial examples. *arXiv preprint arXiv:1802.00420*, 2018.
- Shai Ben-David, John Blitzer, Koby Crammer, Alex Kulesza, Fernando Pereira, and Jennifer Wortman Vaughan. A theory of learning from different domains. *Machine learning*, 79(1-2):151–175, 2010.
- Petra Bevandić, Ivan Krešo, Marin Oršić, and Siniša Šegvić. Discriminative out-of-distribution detection for semantic segmentation. *arXiv preprint arXiv:1808.07703*, 2018.
- Battista Biggio, Igino Corona, Davide Maiorca, Blaine Nelson, Nedim Šrndić, Pavel Laskov, Giorgio Giacinto, and Fabio Roli. Evasion attacks against machine learning at test time. In *Joint European conference on machine learning and knowledge discovery in databases*, pp. 387–402. Springer, 2013.
- Jiefeng Chen, Xi Wu, Vaibhav Rastogi, Yingyu Liang, and Somesh Jha. Robust attribution regularization. In *Advances in Neural Information Processing Systems*, pp. 14300–14310, 2019.
- Hyunsun Choi and Eric Jang. Generative ensembles for robust anomaly detection. 2018.
- M. Cimpoi, S. Maji, I. Kokkinos, S. Mohamed, , and A. Vedaldi. Describing textures in the wild. In *Proceedings of the IEEE Conf. on Computer Vision and Pattern Recognition (CVPR)*, 2014.
- Jesse Davis and Mark Goadrich. The relationship between precision-recall and roc curves. In *Proceedings of the 23rd international conference on Machine learning*, pp. 233–240, 2006.
- Laurent Dinh, Jascha Sohl-Dickstein, and Samy Bengio. Density estimation using real nvp. *arXiv preprint arXiv:1605.08803*, 2016.
- John Duchi, Elad Hazan, and Yoram Singer. Adaptive subgradient methods for online learning and stochastic optimization. *Journal of machine learning research*, 12(Jul):2121–2159, 2011.
- Tom Fawcett. An introduction to roc analysis. *Pattern recognition letters*, 27(8):861–874, 2006.
- Amirata Ghorbani, Abubakar Abid, and James Zou. Interpretation of neural networks is fragile. In *Proceedings of the AAAI Conference on Artificial Intelligence*, volume 33, pp. 3681–3688, 2019.
- Ian J Goodfellow, Jonathon Shlens, and Christian Szegedy. Explaining and harnessing adversarial examples. *arXiv preprint arXiv:1412.6572*, 2014.
- Chuan Guo, Geoff Pleiss, Yu Sun, and Kilian Q Weinberger. On calibration of modern neural networks. In *Proceedings of the 34th International Conference on Machine Learning-Volume 70*, pp. 1321–1330. JMLR. org, 2017.
- Matthias Hein, Maksym Andriushchenko, and Julian Bitterwolf. Why relu networks yield high-confidence predictions far away from the training data and how to mitigate the problem. In *Proceedings of the IEEE Conference on Computer Vision and Pattern Recognition*, pp. 41–50, 2019.
- Dan Hendrycks and Kevin Gimpel. A baseline for detecting misclassified and out-of-distribution examples in neural networks. *arXiv preprint arXiv:1610.02136*, 2016.
- Dan Hendrycks, Mantas Mazeika, and Thomas G Dietterich. Deep anomaly detection with outlier exposure. *arXiv preprint arXiv:1812.04606*, 2018.
- Gao Huang, Zhuang Liu, Laurens Van Der Maaten, and Kilian Q Weinberger. Densely connected convolutional networks. In *Proceedings of the IEEE conference on computer vision and pattern recognition*, pp. 4700–4708, 2017.
- Diederik P Kingma and Jimmy Ba. Adam: A method for stochastic optimization. *arXiv preprint arXiv:1412.6980*, 2014.
- Diederik P Kingma and Max Welling. Auto-encoding variational bayes. *arXiv preprint arXiv:1312.6114*, 2013.
- Alex Krizhevsky, Geoffrey Hinton, et al. Learning multiple layers of features from tiny images. 2009.

- Balaji Lakshminarayanan, Alexander Pritzel, and Charles Blundell. Simple and scalable predictive uncertainty estimation using deep ensembles. In *Advances in neural information processing systems*, pp. 6402–6413, 2017.
- Kimin Lee, Honglak Lee, Kibok Lee, and Jinwoo Shin. Training confidence-calibrated classifiers for detecting out-of-distribution samples. *arXiv preprint arXiv:1711.09325*, 2017.
- Kimin Lee, Kibok Lee, Honglak Lee, and Jinwoo Shin. A simple unified framework for detecting out-of-distribution samples and adversarial attacks. In *Advances in Neural Information Processing Systems*, pp. 7167–7177, 2018.
- Shiyu Liang, Yixuan Li, and Rayadurgam Srikant. Enhancing the reliability of out-of-distribution image detection in neural networks. *arXiv preprint arXiv:1706.02690*, 2017.
- Ilya Loshchilov and Frank Hutter. Sgdr: Stochastic gradient descent with warm restarts. *arXiv preprint arXiv:1608.03983*, 2016.
- Aleksander Madry, Aleksandar Makelov, Ludwig Schmidt, Dimitris Tsipras, and Adrian Vladu. Towards deep learning models resistant to adversarial attacks. *arXiv preprint arXiv:1706.06083*, 2017.
- Andrey Malinin and Mark Gales. Predictive uncertainty estimation via prior networks. In *Advances in Neural Information Processing Systems*, pp. 7047–7058, 2018.
- Christopher D Manning, Christopher D Manning, and Hinrich Schütze. *Foundations of statistical natural language processing*. MIT press, 1999.
- Alexander Meinke and Matthias Hein. Towards neural networks that provably know when they don’t know. *arXiv preprint arXiv:1909.12180*, 2019.
- Sina Mohseni, Mandar Pitale, JBS Yadawa, and Zhangyang Wang. Self-supervised learning for generalizable out-of-distribution detection. 2020.
- Eric Nalisnick, Akihiro Matsukawa, Yee Whye Teh, Dilan Gorur, and Balaji Lakshminarayanan. Do deep generative models know what they don’t know? *arXiv preprint arXiv:1810.09136*, 2018.
- Yuval Netzer, Tao Wang, Adam Coates, Alessandro Bissacco, Bo Wu, and Andrew Y Ng. Reading digits in natural images with unsupervised feature learning. 2011.
- Nicolas Papernot, Patrick McDaniel, Somesh Jha, Matt Fredrikson, Z Berkay Celik, and Ananthram Swami. The limitations of deep learning in adversarial settings. In *2016 IEEE European symposium on security and privacy (EuroS&P)*, pp. 372–387. IEEE, 2016.
- Phillip Pope, Yogesh Balaji, and Soheil Feizi. Adversarial robustness of flow-based generative models. *arXiv preprint arXiv:1911.08654*, 2019.
- Jie Ren, Peter J Liu, Emily Fertig, Jasper Snoek, Ryan Poplin, Mark Depristo, Joshua Dillon, and Balaji Lakshminarayanan. Likelihood ratios for out-of-distribution detection. In *Advances in Neural Information Processing Systems*, pp. 14680–14691, 2019.
- Danilo Jimenez Rezende, Shakir Mohamed, and Daan Wierstra. Stochastic backpropagation and approximate inference in deep generative models. *arXiv preprint arXiv:1401.4082*, 2014.
- Takaya Saito and Marc Rehmsmeier. The precision-recall plot is more informative than the roc plot when evaluating binary classifiers on imbalanced datasets. *PloS one*, 10(3), 2015.
- Vikash Sehwal, Arjun Nitin Bhagoji, Liwei Song, Chawin Sitawarin, Daniel Cullina, Mung Chiang, and Prateek Mittal. Analyzing the robustness of open-world machine learning. In *Proceedings of the 12th ACM Workshop on Artificial Intelligence and Security*, pp. 105–116, 2019.
- Joan Serrà, David Álvarez, Vicenç Gómez, Olga Slizovskaia, José F Núñez, and Jordi Luque. Input complexity and out-of-distribution detection with likelihood-based generative models. *arXiv preprint arXiv:1909.11480*, 2019.
- Johannes Stalldkamp, Marc Schlipsing, Jan Salmen, and Christian Igel. Man vs. computer: Benchmarking machine learning algorithms for traffic sign recognition. *Neural networks*, 32:323–332, 2012.
- Akshayvarun Subramanya, Suraj Srinivas, and R Venkatesh Babu. Confidence estimation in deep neural networks via density modelling. *arXiv preprint arXiv:1707.07013*, 2017.

- Christian Szegedy, Wojciech Zaremba, Ilya Sutskever, Joan Bruna, Dumitru Erhan, Ian Goodfellow, and Rob Fergus. Intriguing properties of neural networks. *arXiv preprint arXiv:1312.6199*, 2013.
- Esteban G Tabak and Cristina V Turner. A family of nonparametric density estimation algorithms. *Communications on Pure and Applied Mathematics*, 66(2):145–164, 2013.
- Antonio Torralba, Rob Fergus, and William T Freeman. 80 million tiny images: A large data set for nonparametric object and scene recognition. *IEEE transactions on pattern analysis and machine intelligence*, 30(11):1958–1970, 2008.
- Aaron Van den Oord, Nal Kalchbrenner, Lasse Espeholt, Oriol Vinyals, Alex Graves, et al. Conditional image generation with pixelcnn decoders. In *Advances in neural information processing systems*, pp. 4790–4798, 2016.
- Pingmei Xu, Krista A Ehinger, Yinda Zhang, Adam Finkelstein, Sanjeev R Kulkarni, and Jianxiong Xiao. Turkergaze: Crowdsourcing saliency with webcam based eye tracking. *arXiv preprint arXiv:1504.06755*, 2015.
- Fisher Yu, Ari Seff, Yinda Zhang, Shuran Song, Thomas Funkhouser, and Jianxiong Xiao. Lsun: Construction of a large-scale image dataset using deep learning with humans in the loop. *arXiv preprint arXiv:1506.03365*, 2015.
- Bolei Zhou, Agata Lapedriza, Aditya Khosla, Aude Oliva, and Antonio Torralba. Places: A 10 million image database for scene recognition. *IEEE transactions on pattern analysis and machine intelligence*, 40(6):1452–1464, 2017.

Supplementary Material

A Proof of Theorem 1

We have

$$R^t(G) = R^t(G^*) + R^t(G) - R^t(G^*) \quad (11)$$

$$= R^t(G^*) + R^s(G) - R^s(G^*) \quad (12)$$

$$+ [(R^t(G) - R^t(G^*)) - (R^s(G) - R^s(G^*))]. \quad (13)$$

The last term is

$$(R^t(G) - R^t(G^*)) - (R^s(G) - R^s(G^*)) \quad (14)$$

$$= (R^t(G) - R^s(G)) - (R^t(G^*) - R^s(G^*)) \quad (15)$$

$$= \frac{1}{2} \mathbb{E}_{x \sim Q_X, y=0} (L(G, x, y; \Omega) - L(G^*, x, y; \Omega)) \quad (16)$$

$$- \frac{1}{2} \mathbb{E}_{x \sim U_X, y=0} (L(G, x, y; \Omega) - L(G^*, x, y; \Omega)) \quad (17)$$

$$= \frac{1}{2} [v(G, G^*; Q_X) - v(G, G^*; U_X)] \quad (18)$$

$$\leq \frac{1}{2} d_G(Q_X, U_X). \quad (19)$$

Therefore,

$$R^t(G) \leq R^t(G^*) + R^s(G) + \frac{1}{2} d_G(Q_X, U_X). \quad (20)$$

Taking inf over $G^* \in \mathcal{G}$ completes the proof.

B More Details of Experiments

B.1 More Experiment Settings

Software and Hardware. We run all experiments with PyTorch and NVIDIA GeForce RTX 2080Ti GPUs.

Number of Evaluation Runs. We run all experiments once with fixed random seeds.

In-distribution Dataset. We provide the details of in-distribution datasets below:

1. **CIFAR-10 and CIFAR-100.** The CIFAR-10 and CIFAR-100 (Krizhevsky et al., 2009) have 10 and 100 classes respectively. Both datasets consist of 50,000 training images and 10,000 test images.
2. **GTSRB.** The German Traffic Sign Recognition Benchmark (GTSRB) (Stallkamp et al., 2012) is a dataset of color images depicting 43 different traffic signs. The images are not of a fixed dimensions and have rich background and varying light conditions as would be expected of photographed images of traffic signs. There are about 34,799 training images, 4,410 validation images and 12,630 test images. We resize each image to 32×32 . The dataset has a large imbalance in the number of sample occurrences across classes. We use data augmentation techniques to enlarge the training data and make the number of samples in each class balanced. We construct a class preserving data augmentation pipeline consisting of rotation, translation, and projection transforms and apply this pipeline to images in the training set until each class contained 10,000 training examples. This new augmented dataset containing 430,000 samples in total is used as $\mathcal{D}_{\text{in}}^{\text{train}}$. We randomly select 10,000 images from original test images as $\mathcal{D}_{\text{in}}^{\text{test}}$.

OOD Test Dataset. We provide the details of OOD test datasets below:

1. **SVHN.** The SVHN dataset Netzer et al. (2011) contains 32×32 color images of house numbers. There are ten classes comprised of the digits 0-9. The original test set has 26,032 images. We randomly select 1,000 images for each class from the test set to form a new test dataset containing 10,000 images for our evaluation.

2. **Textures.** The Describable Textures Dataset (DTD) [Cimpoi et al. \(2014\)](#) contains textural images in the wild. We include the entire collection of 5640 images in DTD and downsample each image to size 32×32 .
3. **Places365.** The Places365 dataset [Zhou et al. \(2017\)](#) contains large-scale photographs of scenes with 365 scene categories. There are 900 images per category in the test set. We randomly sample 10,000 images from the test set for evaluation and downsample each image to size 32×32 .
4. **LSUN (crop) and LSUN (resize).** The Large-scale Scene Understanding dataset (LSUN) has a testing set of 10,000 images of 10 different scenes [Yu et al. \(2015\)](#). We construct two datasets, LSUN-C and LSUN-R, by randomly cropping image patches of size 32×32 and downsampling each image to size 32×32 , respectively.
5. **iSUN.** The iSUN [Xu et al. \(2015\)](#) consists of a subset of SUN images. We include the entire collection of 8925 images in iSUN and downsample each image to size 32×32 .
6. **CIFAR-10.** We use the 10,000 test images of CIFAR-10 as OOD test set for GTSRB.

B.2 Additional Evaluation Metric

AUPR. It is the Area under the Precision-Recall curve, which is another threshold independent metric [Manning et al. \(1999\)](#); [Saito & Rehmsmeier \(2015\)](#). The PR curve is a graph showing the precision= $TP/(TP+FP)$ and recall= $TP/(TP+FN)$ against each other. The metric AUPR-In and AUPR-Out denote the area under the precision-recall curve where in-distribution and out-of-distribution images are specified as positives, respectively.

B.3 Complete Experimental Results

We report the performance of OOD detectors on each of the six OOD test datasets in Table 4 (GTSRB), Table 5 (CIFAR-10) and Table 6 (CIFAR-100).

For different adversarial budget ϵ , We train different models of ADV, AOE and ALOE. The classification performance of the training methods (Original, OE, ADV, AOE, ALOE) under different adversarial budget ϵ is reported in Table 7.

$\mathcal{D}_{\text{out}}^{\text{test}}$	Method	FPR (95% TPR) ↓	Detection Error ↓	AUROC ↑	AUPR In ↑	AUPR Out ↑	FPR (95% TPR) ↓	Detection Error ↓	AUROC ↑	AUPR In ↑	AUPR Out ↑
		without attack					with attack ($\epsilon = 1/255, m = 10$)				
LSUN-C	MSP	0.56	2.04	98.91	98.71	98.53	97.44	33.48	63.00	54.81	59.64
	ODIN	0.75	1.67	99.31	98.70	99.35	81.67	33.45	61.34	51.76	66.21
	Mahalanobis	0.62	2.31	98.56	98.78	95.27	100.00	32.16	68.03	66.47	59.47
	OE	0.00	0.39	99.92	99.94	99.86	26.37	7.65	95.62	96.87	90.88
	OE+ODIN	0.00	0.53	99.92	99.94	99.88	18.91	7.90	96.27	96.16	94.08
	ADV	1.30	2.71	98.78	98.14	98.23	18.94	7.18	94.67	91.79	91.70
	AOE	0.00	0.74	99.83	99.87	99.74	2.47	3.31	98.17	98.44	95.83
	ALOE	0.00	0.60	99.69	99.82	99.26	1.48	2.61	98.79	99.09	96.40
	ALOE+ODIN	0.00	0.62	99.69	99.82	99.28	1.66	2.66	98.70	98.42	96.78
LSUN-R	MSP	0.40	2.01	98.80	98.94	97.99	99.14	21.21	79.90	79.61	68.63
	ODIN	0.39	1.46	99.46	99.28	99.36	73.00	18.67	85.16	80.80	80.06
	Mahalanobis	0.49	2.39	98.63	99.14	95.31	100.00	23.18	78.17	81.15	66.47
	OE	0.00	0.17	99.98	99.98	99.96	4.68	3.86	97.89	98.63	95.38
	OE+ODIN	0.00	0.15	99.98	99.98	99.97	1.62	3.19	98.88	99.21	98.05
	ADV	0.79	2.52	99.02	98.60	98.44	12.30	5.87	96.07	95.16	92.19
	AOE	0.00	0.38	99.90	99.93	99.82	0.00	1.16	98.78	99.31	96.34
	ALOE	0.00	0.26	99.86	99.90	99.78	0.00	0.95	99.35	99.63	97.73
	ALOE+ODIN	0.00	0.26	99.86	99.90	99.79	0.00	0.88	99.47	99.69	98.17
iSUN	MSP	0.82	2.23	98.52	98.06	97.82	98.86	21.56	79.19	77.18	68.38
	ODIN	0.92	1.76	99.09	98.07	99.12	72.71	19.46	83.94	77.86	79.35
	Mahalanobis	0.61	2.44	98.63	99.03	95.25	100.00	23.26	78.52	80.81	67.24
	OE	0.00	0.13	99.98	99.98	99.97	5.48	3.89	97.76	98.56	95.08
	OE+ODIN	0.00	0.12	99.98	99.98	99.98	1.73	3.18	98.80	99.16	97.87
	ADV	1.54	2.97	98.66	98.05	98.06	16.21	6.77	94.98	92.41	91.08
	AOE	0.00	0.40	99.90	99.92	99.83	0.02	1.18	98.76	99.30	96.27
	ALOE	0.00	0.25	99.82	99.88	99.71	0.00	0.95	99.29	99.60	97.40
	ALOE+ODIN	0.00	0.24	99.83	99.88	99.73	0.00	0.87	99.41	99.66	97.88
Textures	MSP	3.85	3.96	96.65	91.11	97.41	93.14	29.10	67.90	58.35	65.24
	ODIN	5.05	4.19	96.22	89.46	97.62	73.74	28.80	67.07	55.61	72.70
	Mahalanobis	3.03	3.83	97.39	94.24	94.78	100.00	32.98	66.53	59.58	61.13
	OE	0.12	0.66	99.82	99.39	99.81	39.15	7.26	94.99	95.91	89.18
	OE+ODIN	0.12	0.64	99.80	99.21	99.81	19.98	6.99	96.21	96.07	93.32
	ADV	3.07	3.83	97.59	94.18	97.60	26.49	9.02	92.28	85.94	90.03
	AOE	0.02	0.90	99.79	99.71	99.69	4.93	4.84	97.43	97.06	95.18
	ALOE	0.02	0.75	99.70	99.68	99.40	2.23	3.13	98.44	98.32	96.17
	ALOE+ODIN	0.04	0.78	99.68	99.60	99.38	2.27	3.24	98.23	96.89	96.53
Places365	MSP	0.60	2.11	98.91	98.94	98.47	98.59	24.28	76.10	72.14	66.47
	ODIN	0.52	1.65	99.44	99.19	99.43	76.28	22.74	79.77	71.52	76.74
	Mahalanobis	1.45	3.08	98.25	98.56	94.86	100.00	33.47	65.85	65.73	56.85
	OE	0.00	0.31	99.93	99.94	99.87	37.96	6.25	95.23	97.08	88.37
	OE+ODIN	0.00	0.34	99.93	99.95	99.88	20.40	6.05	96.54	97.66	92.40
	ADV	0.73	2.43	99.06	98.98	98.46	15.73	6.08	95.82	95.38	91.72
	AOE	0.00	0.66	99.88	99.91	99.81	0.70	2.28	98.49	99.07	95.75
	ALOE	0.00	0.40	99.75	99.85	99.48	0.11	1.54	98.94	99.37	96.38
	ALOE+ODIN	0.00	0.41	99.75	99.85	99.47	0.10	1.53	99.06	99.42	96.86
CIFAR-10	MSP	0.56	2.16	98.91	98.82	98.57	98.39	26.51	73.53	67.90	65.11
	ODIN	0.89	1.84	99.31	98.89	99.32	78.25	26.08	75.16	65.33	73.79
	Mahalanobis	1.68	3.15	98.26	98.43	94.96	100.00	33.83	65.62	64.05	57.25
	OE	0.00	0.36	99.92	99.94	99.85	41.45	6.49	95.07	96.97	88.26
	OE+ODIN	0.00	0.37	99.92	99.94	99.86	22.18	6.25	96.39	97.58	92.26
	ADV	1.28	2.84	98.83	98.72	98.24	18.08	6.77	95.14	93.76	91.14
	AOE	0.00	0.64	99.88	99.91	99.80	0.80	2.52	98.47	99.03	95.73
	ALOE	0.00	0.39	99.73	99.84	99.41	0.12	1.63	98.91	99.36	96.27
	ALOE+ODIN	0.00	0.39	99.73	99.84	99.39	0.14	1.64	99.03	99.41	96.77

Table 4: Distinguishing in- and out-of-distribution test set data for image classification. We use GTSRB as $\mathcal{D}_{\text{in}}^{\text{test}}$. We contrast performance on clean images (without attack) and PGD attacked images. All values are percentages. \uparrow indicates larger value is better, and \downarrow indicates lower value is better.

$\mathcal{D}_{\text{out}}^{\text{test}}$	Method	FPR (95% TPR) ↓	Detection Error ↓	AUROC ↑	AUPR In ↑	AUPR Out ↑	FPR (95% TPR) ↓	Detection Error ↓	AUROC ↑	AUPR In ↑	AUPR Out ↑
		without attack					with attack ($\epsilon = 1/255, m = 10$)				
LSUN-C	MSP	36.19	9.77	95.26	96.31	93.90	99.94	50.00	9.51	31.03	32.63
	ODIN	5.81	5.18	98.82	98.90	98.74	97.86	49.89	24.90	35.59	37.22
	Mahalanobis	1.86	3.00	99.39	99.21	99.40	80.16	34.23	66.35	57.16	68.36
	OE	0.95	2.67	99.41	99.54	99.21	99.98	50.00	28.11	36.77	37.08
	OE+ODIN	1.89	3.08	99.38	99.43	99.27	99.39	50.00	37.60	39.99	43.25
	ADV	55.91	16.43	90.38	91.86	88.32	91.72	26.45	75.32	80.75	66.49
	AOE	4.99	4.87	98.86	99.00	98.66	71.17	21.76	84.96	86.67	81.13
	ALOE	3.44	4.20	98.81	99.06	98.37	43.55	12.02	93.30	94.91	88.51
	ALOE+ODIN	2.50	3.73	99.07	99.25	98.72	31.21	10.60	94.83	95.76	92.24
LSUN-R	MSP	37.09	10.13	95.09	96.20	93.55	100.00	50.00	20.08	34.63	34.44
	ODIN	2.02	3.23	99.50	99.53	99.47	83.12	39.82	63.22	58.83	64.96
	Mahalanobis	5.90	5.33	98.44	98.12	98.55	86.18	42.69	52.53	46.99	58.85
	OE	2.57	3.74	98.87	99.14	98.34	100.00	50.00	30.89	38.12	37.99
	OE+ODIN	1.07	2.65	99.35	99.45	99.09	98.84	45.45	48.59	45.55	49.45
	ADV	66.89	18.41	88.10	90.34	84.73	99.88	30.56	67.79	76.04	56.30
	AOE	8.22	5.65	98.07	98.52	96.85	93.86	22.07	81.96	85.85	71.77
	ALOE	4.90	4.76	98.49	98.78	97.86	60.94	13.85	91.32	93.35	84.49
	ALOE+ODIN	3.47	4.16	98.74	98.97	98.18	46.37	12.16	92.96	94.20	88.45
iSUN	MSP	40.11	10.54	94.72	96.08	92.85	99.97	50.00	20.01	34.14	34.58
	ODIN	2.96	3.74	99.35	99.39	99.33	81.11	40.73	60.54	54.68	64.68
	Mahalanobis	9.56	7.13	97.62	97.07	97.91	80.92	41.57	50.74	45.57	60.91
	OE	2.94	3.91	98.86	99.12	98.37	100.00	50.00	30.56	38.98	36.8
	OE+ODIN	1.14	2.65	99.31	99.43	99.04	98.76	45.91	47.43	44.74	49.13
	ADV	70.28	20.83	85.85	88.22	81.86	99.95	33.18	64.91	72.04	54.61
	AOE	9.23	5.94	97.91	98.36	96.78	94.25	23.01	81.09	85.24	70.20
	ALOE	6.03	5.45	98.32	98.62	97.70	63.64	14.94	90.49	92.20	84.45
	ALOE+ODIN	4.91	4.79	98.57	98.83	98.00	9.74	13.18	92.10	93.26	87.75
Textures	MSP	67.17	19.11	86.99	86.07	83.04	99.98	50.00	5.09	31.35	30.95
	ODIN	57.36	22.97	84.80	82.60	84.76	98.60	49.96	11.69	32.47	32.71
	Mahalanobis	45.71	23.08	82.67	73.78	86.30	91.31	47.31	17.88	34.27	40.91
	OE	6.05	5.28	98.43	98.67	98.01	99.96	50.00	28.04	36.33	37.74
	OE+ODIN	6.74	5.69	97.58	96.56	97.88	97.47	45.70	38.44	40.27	47.00
	ADV	70.83	20.97	85.40	86.96	81.00	99.20	34.67	63.21	69.27	52.76
	AOE	9.23	5.94	97.91	98.36	96.78	92.20	32.23	71.22	71.12	64.18
	ALOE	4.57	4.66	98.67	98.87	98.32	40.09	13.18	92.65	93.27	89.25
	ALOE+ODIN	3.78	4.36	98.77	98.87	98.56	30.01	12.11	93.64	93.23	92.23
Places365	MSP	63.69	17.90	88.42	88.19	85.04	100.00	50.00	2.15	30.49	31.17
	ODIN	63.69	17.90	88.42	88.19	85.04	100.00	50.00	6.43	31.32	31.34
	Mahalanobis	90.84	41.73	60.90	59.08	58.92	99.94	50.00	0.73	30.77	30.70
	OE	10.21	7.22	97.11	96.73	97.00	100.00	50.00	13.72	32.25	33.11
	OE+ODIN	10.71	7.70	96.91	96.43	96.96	99.73	50.00	19.94	34.28	34.83
	ADV	66.66	19.72	86.72	87.37	84.03	99.94	33.78	63.32	69.87	52.44
	AOE	16.20	8.88	96.32	95.97	96.07	95.88	30.54	72.52	72.92	63.59
	ALOE	10.21	7.43	97.13	96.59	97.20	55.35	17.90	88.05	87.11	83.81
	ALOE+ODIN	9.37	7.02	97.27	96.69	97.35	46.94	16.52	89.23	87.40	87.17
SVHN	MSP	65.77	16.90	89.19	90.53	85.45	99.99	50.00	5.23	31.27	31.07
	ODIN	43.04	17.13	90.45	90.23	90.19	100.00	50.00	3.95	30.98	31.03
	Mahalanobis	32.20	14.06	92.16	90.56	90.98	100.00	50.00	7.04	31.55	31.33
	OE	4.09	4.21	98.55	98.92	97.95	100.00	50.00	19.47	33.71	34.53
	OE+ODIN	3.50	4.08	98.76	98.85	98.53	99.95	50.00	13.73	32.86	32.80
	ADV	71.37	18.99	86.90	89.17	82.59	99.97	31.70	65.85	74.42	53.86
	AOE	10.13	6.58	98.08	98.36	97.52	86.10	26.51	78.57	82.16	70.23
	ALOE	3.65	4.30	98.62	98.93	98.08	60.40	13.28	91.74	93.85	85.84
	ALOE+ODIN	2.85	3.88	98.87	99.12	98.41	45.26	11.79	93.35	94.74	89.72

Table 5: Distinguishing in- and out-of-distribution test set data for image classification. We use CIFAR-10 as $\mathcal{D}_{\text{in}}^{\text{test}}$. We contrast performance on clean images (without attack) and PGD attacked images. All values are percentages. \uparrow indicates larger value is better, and \downarrow indicates lower value is better.

$\mathcal{D}_{\text{out}}^{\text{test}}$	Method	FPR (95% TPR)	Detection Error	AUROC	AUPR In	AUPR Out	FPR (95% TPR)	Detection Error	AUROC	AUPR In	AUPR Out
		↓	↑		↑	↑	↓	↓	↑	↑	↑
		without attack					with attack ($\epsilon = 1/255, m = 10$)				
LSUN-C	MSP	66.06	24.67	83.33	85.59	81.34	100.00	50.00	6.84	31.83	30.96
	ODIN	14.33	8.56	97.36	97.52	97.24	94.06	49.23	45.63	45.02	49.14
	Mahalanobis	1.10	2.26	99.63	99.46	99.58	89.58	38.18	59.86	52.20	60.62
	OE	23.20	10.68	95.80	96.26	95.38	100.00	50.00	5.19	30.90	31.43
	OE+ODIN	20.25	9.97	96.54	96.87	96.40	98.97	50.00	27.62	36.93	36.89
	ADV	72.85	26.85	80.69	82.59	78.77	97.89	39.09	55.92	64.86	49.38
	AOE	35.00	14.88	92.98	93.41	92.78	86.88	34.75	69.36	72.96	65.65
	ALOE	40.06	15.40	92.27	92.76	91.76	79.72	29.69	76.68	78.83	73.99
LSUN-R	ALOE+ODIN	30.60	12.79	94.35	94.77	93.94	70.76	25.02	82.50	84.18	80.40
	MSP	86.39	39.29	64.99	65.31	63.50	100.00	50.00	1.52	30.83	30.74
	ODIN	52.71	20.65	87.50	88.00	86.41	99.68	50.00	26.14	36.25	36.23
	Mahalanobis	24.55	13.48	92.07	88.74	93.43	96.11	49.73	20.17	34.65	37.65
	OE	64.82	22.67	84.73	85.92	82.25	100.00	50.00	3.50	31.36	30.57
	OE+ODIN	47.49	17.82	90.24	91.11	89.18	99.75	50.00	25.91	36.14	36.08
	ADV	87.97	34.90	69.68	72.27	65.85	99.95	46.18	38.57	50.67	40.22
	AOE	62.83	26.76	81.20	80.77	81.64	96.09	47.04	51.10	54.15	49.10
iSUN	ALOE	67.72	28.13	78.94	78.09	78.45	94.37	45.67	55.25	55.79	53.05
	ALOE+ODIN	64.15	25.97	81.35	80.35	81.12	91.41	42.00	60.40	59.58	58.18
	MSP	87.37	41.04	62.77	62.59	61.74	100.00	50.00	1.45	30.80	30.75
	ODIN	58.69	22.59	85.41	86.12	83.94	99.73	50.00	23.99	35.45	35.51
	Mahalanobis	29.67	16.06	89.60	84.71	91.85	91.72	48.10	23.32	35.55	42.45
	OE	67.22	23.85	83.55	84.73	81.24	100.00	50.00	3.12	30.48	31.36
	OE+ODIN	51.00	18.70	89.30	90.17	88.09	99.79	50.00	24.35	35.58	35.57
	ADV	90.41	38.17	65.51	67.77	61.46	100.00	48.66	35.47	46.06	39.18
Textures	AOE	69.41	29.68	77.58	76.65	77.97	97.77	48.72	47.20	50.46	46.04
	ALOE	73.38	31.01	74.92	72.04	75.35	95.98	47.81	51.36	51.59	49.83
	ALOE+ODIN	70.22	28.84	77.54	75.28	77.39	93.31	44.55	56.52	55.08	54.63
	MSP	86.30	33.84	70.04	68.83	65.87	100.00	50.00	1.59	32.50	29.11
	ODIN	83.60	35.06	68.91	64.47	67.88	99.76	49.97	10.26	32.02	31.97
	Mahalanobis	83.85	44.25	35.19	38.84	52.04	97.32	49.17	3.97	31.43	33.13
	OE	63.08	22.15	85.39	86.82	83.21	99.98	50.00	3.66	30.67	31.30
	OE+ODIN	61.55	23.08	85.02	85.47	84.43	98.46	50.00	19.31	34.05	34.71
Places365	ADV	90.25	36.37	66.67	64.54	62.80	100.00	48.40	36.48	46.66	38.01
	AOE	62.95	23.49	83.91	84.04	82.84	96.21	44.59	51.13	55.81	48.67
	ALOE	59.25	23.14	85.08	85.71	84.22	90.06	40.34	62.16	65.62	59.16
	ALOE+ODIN	57.27	21.45	86.58	86.91	85.93	86.61	36.97	67.10	69.31	64.52
	MSP	83.43	31.46	74.09	75.41	70.01	100.00	50.00	0.81	30.78	30.68
	ODIN	81.11	29.97	76.00	76.35	72.17	99.99	50.00	9.25	31.73	31.82
	Mahalanobis	96.21	49.23	49.43	50.26	48.72	99.99	50.00	0.10	30.69	30.69
	OE	60.69	20.69	86.70	87.52	84.63	100.00	50.00	1.03	30.73	30.76
SVHN	OE+ODIN	62.94	20.06	87.09	88.42	84.61	99.99	50.00	12.36	32.31	32.45
	ADV	84.38	31.96	73.73	75.76	70.26	99.99	44.52	40.04	53.00	40.77
	AOE	57.94	22.57	85.71	86.01	85.05	98.11	43.09	52.73	59.26	47.92
	ALOE	55.00	21.73	86.64	87.00	86.11	92.55	38.69	64.07	68.39	58.54
	ALOE+ODIN	52.38	19.04	88.94	89.84	87.74	89.91	33.68	70.14	74.05	64.14
	MSP	80.76	30.44	76.14	79.56	72.24	100.00	50.00	2.14	31.29	30.39
	ODIN	62.61	20.82	86.59	88.44	84.26	99.97	50.00	10.87	31.99	32.18
	Mahalanobis	87.09	40.52	59.18	53.01	60.18	100.00	50.00	0.10	30.69	30.69
GTSRB	OE	59.92	16.27	90.21	92.39	86.23	100.00	50.00	1.12	30.88	30.62
	OE+ODIN	42.32	14.71	92.64	93.68	91.45	100.00	50.00	10.58	31.97	32.10
	ADV	86.94	30.78	74.31	78.72	69.08	100.00	42.29	41.58	57.07	41.29
	AOE	71.87	20.80	86.04	88.70	81.25	99.68	40.22	51.28	63.00	45.85
	ALOE	76.54	21.96	84.46	87.58	77.98	99.39	38.32	57.69	67.38	49.78
	ALOE+ODIN	76.27	20.18	85.75	88.88	79.27	99.00	34.98	62.99	71.53	53.43

Table 6: Distinguishing in- and out-of-distribution test set data for image classification. We use CIFAR-100 as $\mathcal{D}_{\text{in}}^{\text{test}}$. We contrast performance on clean images (without attack) and PGD attacked images. All values are percentages. \uparrow indicates larger value is better, and \downarrow indicates lower value is better.

$\mathcal{D}_{\text{in}}^{\text{test}}$	Method	$\epsilon = 2/255$		$\epsilon = 3/255$		$\epsilon = 4/255$	
		Accuracy	Robustness	Accuracy	Robustness	Accuracy	Robustness
GTSRB	Original	99.33%	65.46%	99.33%	47.91%	99.33%	47.20%
	OE	99.38%	57.76%	99.38%	38.48%	99.38%	38.20%
	ADV	98.50%	93.01%	96.58%	88.04%	96.13%	87.79%
	AOE	97.90%	82.87%	95.32%	68.88%	95.27%	64.16%
	ALOE	98.20%	82.76%	95.12%	63.41%	95.14%	60.97%
CIFAR-10	Original	94.08%	2.17%	94.08%	0.10%	94.08%	0.09%
	OE	94.59%	4.28%	94.59%	0.78%	94.59%	0.71%
	ADV	91.20%	77.35%	90.10%	70.81%	89.93%	70.33%
	AOE	92.56%	70.58%	87.13%	66.35%	89.76%	69.82%
	ALOE	92.58%	75.64%	90.84%	67.66%	90.90%	69.63%

Table 7: The classification accuracy and robustness of different models with various adversarial budget ϵ . *Robustness* measures the accuracy under PGD attack with number of attack steps of 10.